

Supporting information

## **Cone-spiral magnetic ordering dominated lattice distortion and giant negative thermal expansion in Fe-doped MnNiGe compounds**

Feiran Shen<sup>‡,abc</sup>, Houbo Zhou<sup>‡,ab</sup>, Fengxia Hu,<sup>\*abd</sup> Jian-Tao Wang,<sup>abd</sup> Sihao Deng,<sup>c</sup> Baotian Wang,<sup>c</sup> Hui Wu,<sup>e</sup> Qingzhen Huang,<sup>e</sup> Jing Wang,<sup>\*abf</sup> Jie Chen,<sup>c</sup> Lunhua He,<sup>\*acd</sup> Jiazheng Hao,<sup>a</sup> Zibing Yu,<sup>ab</sup> Feixiang Liang,<sup>ab</sup> Tianjiao Liang,<sup>c</sup> Jirong Sun,<sup>abd</sup> and Baogen Shen<sup>\*abd</sup>

<sup>a</sup>Institute of Physics, Chinese Academy of Sciences, Beijing 100190, P. R. China.

<sup>b</sup>School of Physical Sciences, University of Chinese Academy of Sciences, Beijing 101408, China.

<sup>c</sup>Spallation Neutron Source Science Center, Dongguan 523803, China.

<sup>d</sup>Songshan Lake Materials Laboratory, Dongguan, Guangdong 523808, P. R. China.

<sup>e</sup>NIST Center for Neutron Research, National Institute of Standards and Technology, Gaithersburg, Maryland 20899, USA.

<sup>f</sup>Fujian Innovation Academy, Chinese Academy of Sciences, Fuzhou, Fujian 350108, China.

\*To whom correspondence should be addressed. E-mail: fxhu@iphy.ac.cn; lhhe@iphy.ac.cn; wangjing@iphy.ac.cn, shenbg@iphy.ac.cn

‡ These authors contribute equally to this work.

### **Series title:**

**I. Table S1, sample preparation, characterization, and computational methods of first-principles calculations**

**II. Magnetic and crystal structure studied by Neutron powder diffraction (NPD)**

**III. The intrinsic crystallographic change during phase transition**

**IV. Texture effect studied by XRD**

**V. Numerical simulation of the enhanced  $\Delta L/L$**

**VI. Broadening of NTE temperature range for bonded samples**

**VII. Enhancements of NTE studied in a single composition**

**I. Table S1**

Magnetostructural transition temperature ( $T_{\text{mstru}}$ ), Magnetic structure, magnetic moment, atomic distance  $d_1$  between Mn1-Mn2, atomic distance  $d_2$  between Mn2-Mn3, angle  $\text{agl}_M$  of Mn2-Mn3-Mn4 atomic chain, lattice parameters, variation of lattice parameters and volume across the  $T_{\text{mstru}}$ , linear  $(\Delta L/L)_0 = (\Delta V/V)/3$  from crystallographic value in the temperature interval  $(\Delta T)_0$ , measured  $\Delta L/L$  for the bonded samples in the temperature interval  $\Delta T$  and obtained NTE coefficient  $\bar{\alpha}$  accordingly, enhanced  $\Delta L/L$  compared to  $(\Delta L/L)_0$   $[(\Delta L/L)/(\Delta L/L)_0]$ , orientation coefficient OC of different crystal plane of hexagonal structure, for the Fe-doped MnNiGe alloys in comparison to  $\text{MnCoGe}_{0.99}\text{In}_{0.01}$ .

	$\text{Mn}_{0.87}\text{Fe}_{0.13}\text{NiGe}$ (Ni1)	$\text{MnCoGe}_{0.99}\text{In}_{0.01}$ (Co1)	Diff	$\text{MnNi}_{0.8}\text{Fe}_{0.2}\text{Ge}$ (Ni2)	$\text{MnNi}_{0.77}\text{Fe}_{0.23}\text{Ge}$ (Ni3)	$\text{Mn}_{0.91}\text{Fe}_{0.09}\text{NiGe}$ (Ni4)	$\text{Mn}_{0.89}\text{Fe}_{0.11}\text{NiGe}$ (Ni5)
$T_{\text{mstru}}$	256K	308K	-	310K	295K	308K	277K
Magn <sub>ort</sub>	Cone-spiral	Linear FM	-	Cone-spiral	Cone-spiral	Cone-spiral	Cone-spiral
$M_{\text{Mn}}(\mu_B)$	2.66(1) (200K)	2.74(5) (250K)	-	-	-	-	2.57(3) (180K)
Angle from a-axis	70°(200K)	along c-axis	-	-	-	-	80°(180K)
T	250K	300K	-	295K	295K	295K	277K
$d_1(\text{Å})$	3.204(7)	3.324(8)	-3.61%	3.235(5)	3.26(1)	3.213(3)	3.212(8)
$d_2(\text{Å})$	3.152(8)	3.072(2)	2.60%	3.167(2)	3.157(5)	3.155(1)	3.150(3)
$\text{agl}_M$ (°)	144.3(5)	148.6(4)	-2.89%	145.0(2)	145.9(5)	144.9(1)	144.8(3)
$a_0(\text{Å})$	6.0016(1)	5.9165(2)	1.44%	6.0408(1)	6.0350(2)	6.0152(1)	6.0049(1)
$b_0(\text{Å})$	3.7427(1)	3.8307(2)	-2.35%	3.7844(1)	3.7840(1)	3.7510(1)	3.7456(1)
$c_0(\text{Å})$	7.0869(1)	7.0639(3)	0.33%	7.1089(1)	7.1117(3)	7.0862(3)	7.0831(2)
$a_H(\text{Å})$	4.0867(1)	4.0897(1)	-0.07%	4.0996(2)	4.1020(1)	4.0870(3)	4.0868(1)
$c_H(\text{Å})$	5.3581(2)	5.3158(3)	0.80%	5.3923(9)	5.3848(1)	5.3793(8)	5.3709(2)
$\Delta c_H - a_0$ (%)	12.01	11.30	6.28%	12.02	12.07	11.82	11.80
$\Delta a_H - b_0$ (%)	-9.19	-6.76	-35.95%	-8.33	-8.40	-8.96	-8.34
$\Delta V/V$ (%)	-2.63	-3.92	-32.91%	-3.53	-3.49	-2.66	-2.53
$\Delta \text{anis}$ (%)	8.68	7.49	15.89%	8.35	8.40	8.51	8.27
wRp (%)	7.97	9.43	-	3.63	3.78	4.45	4.09
CHI <sup>2</sup>	2.23	0.86	-	1.17	1.30	1.83	3.35
$(\Delta L/L)_0$ ( $10^{-6}$ )	7121	10995		7473	7626	7190	
$(\Delta T)_0$	40K(240-280K)	60K(270-330K)		35K(295-330K)	35K(275-310K)	50K(285-335K)	
$\Delta L/L$ ( $10^{-6}$ )	23690	10231		17416	16172	9171	
$\Delta T$	195K(80-275K)	108K(192-310K)		162K(180-342K)	186K(132-318K)	138K(194-332K)	
$\bar{\alpha}$	$-121.5 \times 10^{-6}/\text{K}$	$-94.7 \times 10^{-6}/\text{K}$		$-107.5 \times 10^{-6}/\text{K}$	$-86.9 \times 10^{-6}/\text{K}$	$-66.5 \times 10^{-6}/\text{K}$	
$(\Delta L/L)/(\Delta L/L)_0$	3.33	0.93		2.33	2.12	1.28	
OC(110)	1.93	0.92		1.69	1.95	1.36	
OC(002)	1.23	1.10		0.96	1.40	1.22	
OC(102)	0.42	1.00		0.71	0.46	0.65	
OC(112)	0.58	0.94		1.19	0.65	1.00	
OC(202)	0.84	1.04		0.44	0.54	0.77	

\*The subscripts O, H denote orthorhombic, hexagonal structure, respectively.

### Sample preparation

The employed MnNiGe-based compounds, i.e.  $\text{Mn}_{1-x}\text{Fe}_x\text{NiGe}$  ( $x = 0.09, 0.11, 0.13$ ),  $\text{MnNi}_{1-y}\text{Fe}_y\text{Ge}$  ( $y = 0.20, 0.23$ ), were fabricated by conventional arc melting technique followed by annealing at 875 °C for 6 days, and then quenching in liquid nitrogen. The as-quenched ingots have naturally cracked into powders, which were further milled by hand in agate mortar into particle series with different sizes by controlling milling time, so as to control the texture effect under pressure. Because the sample is brittle and very easy to be cracked. The milling time by hand ranging from 5min to 10min is enough to control the particle size required in this work. Then, a few epoxy plus hardening agent, totally 3–4 wt%, was introduced and evenly mixed with the

powders. The mixtures were molded under pressure about 1.35 GPa and then solidified at 170 °C, eventually resulted in the bonded pellets.

### Characterization

The linear thermal expansion data  $\Delta L/L$  were measured using high-resolution strain gauge. Magnetic measurements were performed using a superconducting quantum interference magnetometer (SQUID-VSM). The morphology of particle was examined by Helios Nanolab 600I Scanning Electron Microscope (SEM). Neutron powder diffraction (NPD) was performed at the NIST Center for Neutron Research on the BT-1 high-resolution neutron powder diffractometer, and time-of-flight (TOF) general purpose powder diffractometer (GPPD) at China Spallation Neutron Source (CSNS). At BT-1, Ge(311) monochromator was used to produce a monochromatic neutron beam of wavelength 2.0775 Å. While at GPPD, neutron diffraction patterns were collected with wavelength band from 0.1 to 8.8 Å. The variable temperature x-ray diffraction (XRD) was performed at Rigaku-SmartLab X-ray diffractometer. The crystal and magnetic structures were refined by the Rietveld method using the General Structure Analysis System (GSAS) suite and the FullProf suite of programs.

### Computational methods of first-principles calculations

The density functional theory (DFT) calculations are performed using the Vienna *ab initio* simulation package (VASP) [G. Kresse, et al, *Phys. Rev. B*, 1993, **47**, 558; G. Kresse, et al, *Phys. Rev. B*, 1996, **54**, 11169] with the projector augmented wave method [P. E. Blöchl, *Phys. Rev. B* 1994, **50**, 17953; G. Kresse et al, *Phys. Rev. B*, 1999, **59**, 1758] and spin polarized generalized gradient approximation [Ref. 38] for the exchange-correlation energy. The valence states 3d<sup>6</sup>4s<sup>1</sup> for Mn, 3d<sup>7</sup>4s<sup>1</sup> for Fe, 3d<sup>9</sup>4s<sup>1</sup> for Ni, and 4s<sup>2</sup>4p<sup>2</sup> for Ge are used with the energy cutoff of 400 eV for the plane wave basis set. The ternary MnNiGe has a 12 atoms unit cell, including 4 Mn, 4 Ni, and 4 Ge atoms, occupying the *4c* crystallographic positions. To simulate the cone-spiral and spiral AFM magnetic structures in Mn<sub>0.87</sub>Fe<sub>0.13</sub>NiGe compound, a 6 × 1 × 1 supercell (including 21 Mn, 3 Fe, 24 Ni and 24 Ge atoms) is adopted with the experimental lattice parameters ( $a=36.0034$  Å,  $b=3.7327$  Å, and  $c= 7.0836$  Å), crystallographic positions and magnetic configurations obtained by the NPD data (see Table S1). The Brillouin zone is sampled with a 1 × 12 × 6 Gamma-centered *k*-point grid. The energy convergence criterion is set at 10<sup>-5</sup> eV throughout the present calculations. The lattice compression and expansion are simulated with an isotropic lattice strain from -5% to +5% related to the experimental lattice parameters.

## II. Magnetic and crystal structure studied by Neutron powder diffraction (NPD)

Due to the introduction of Fe, all the Fe-doped MnNiGe, i.e. Mn<sub>1-x</sub>Fe<sub>x</sub>NiGe ( $x = 0.09, 0.11, 0.13$ ), MnNi<sub>1-y</sub>Fe<sub>y</sub>Ge ( $y = 0.20, 0.23$ ) undergo concurrent magnetic and structural transition, the so-called magnetostructural transition,  $T_{mstru}$ , which locates at 308K, 277K, 256K, 310K, 295K, respectively. For MnCoGe<sub>0.99</sub>In<sub>0.01</sub>, its  $T_{mstru}$  locates at 308K. The details are listed in **Table S1**.

To know the details of magnetic and crystal structure during phase transition, we performed variable temperature NPD or XRD studies on the free particles. Careful refinements reveal that the lattice distortion during phase transition of Fe-doped MnNiGe alloys is more significant than that of MnCoGe-based alloys because of the distinct magnetic coupling in martensite. Typically, **Fig. S1** presents the compared change of magnetic and crystal structure during the magnetostructural phase transition between Mn<sub>0.87</sub>Ni<sub>0.13</sub>FeGe and MnCoGe<sub>0.99</sub>In<sub>0.01</sub>, where the fragments of cone-spiral magnetic structure (Mn<sub>0.87</sub>Fe<sub>0.13</sub>NiGe) and linear FM (MnCoGe<sub>0.99</sub>In<sub>0.01</sub>) structure in martensite viewed along the *b* axes with selected distances labeled in Å are denoted. The Mn1-

Mn2 atoms separated by the distance  $d_1$  along c-axis, and the Mn2-Mn3 atoms separated by the distance  $d_2$ , and the angle  $agl_M$  of Mn2-Mn3-Mn4 atomic chain are also indicated.

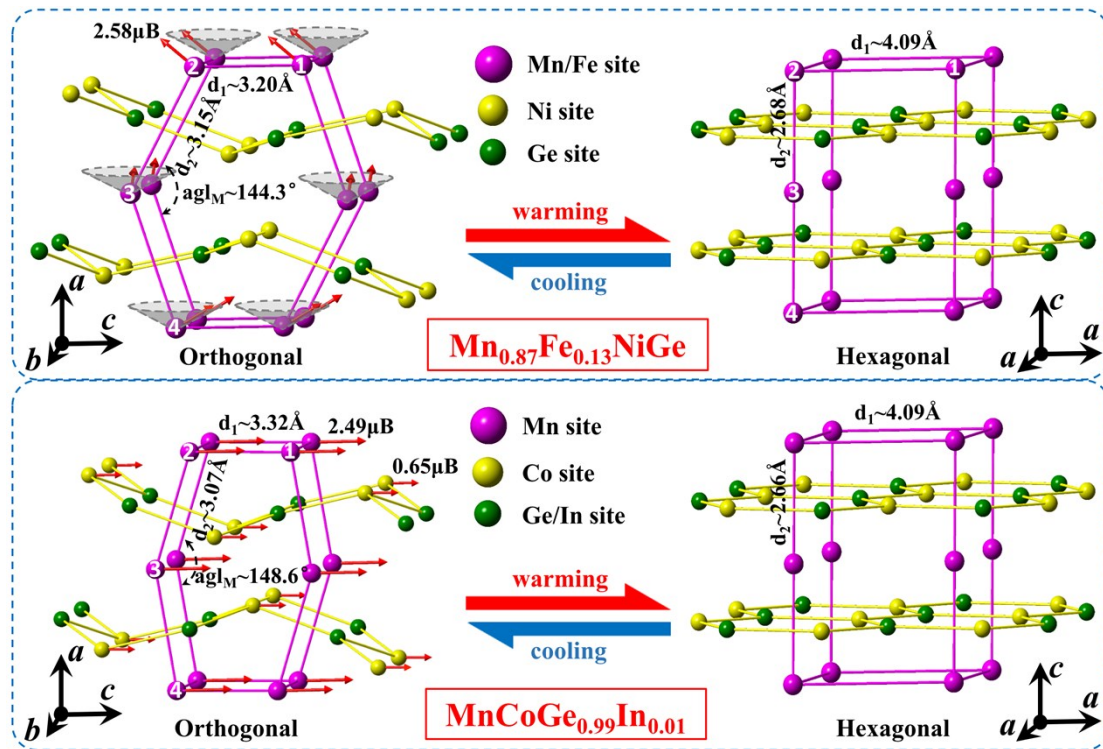


**Fig. S1** The compared change of magnetic and crystal structure during the phase transition between  $Mn_{0.87}Ni_{0.13}FeGe$  (at 250K) and  $MnCoGe_{0.99}In_{0.01}$  (at 300K), where fragments of the cone-spiral magnetic structure ( $Mn_{0.87}Fe_{0.13}NiGe$ ) and linear FM ( $MnCoGe_{0.99}In_{0.01}$ ) structure in martensite viewed along the b axes with selected distances labeled in Å are denoted. The Mn1-Mn2 atoms separated by the distance  $d_1$  along c-axis, and the Mn2-Mn3 atoms separated by the distance  $d_2$ , and the angle  $agl_M$  of Mn2-Mn3-Mn4 atomic chain are also indicated.

Moreover, **Fig. S2** typically displays the refined lattice parameters of hexagonal and orthorhombic structure for  $Mn_{0.87}Ni_{0.13}FeGe$  compared to  $MnCoGe_{0.99}In_{0.01}$ . For the former with cone-spiral magnetic structure in martensite, the hexagonal lattice expands along the c-axis by 12.01% and contracts along the a-axis by 9.19% on cooling, while for the latter with linear FM structure in martensite, the hexagonal lattice expands along the c-axis by 11.3% and contracts along the a-axis by 6.8%. Calculations indicate that the degree of lattice distortion of  $Mn_{0.87}Ni_{0.13}FeGe$ ,  $\Delta_{ani} \sim 8.68\%$ , is larger than that of  $MnCoGe_{0.99}In_{0.01}$ ,  $\Delta_{ani} \sim 7.49\%$ , though the former shows smaller  $-\Delta V/V \sim 2.63\%$  than the latter ( $-\Delta V/V \sim 3.92\%$ ), as shown in **Fig. S2**.

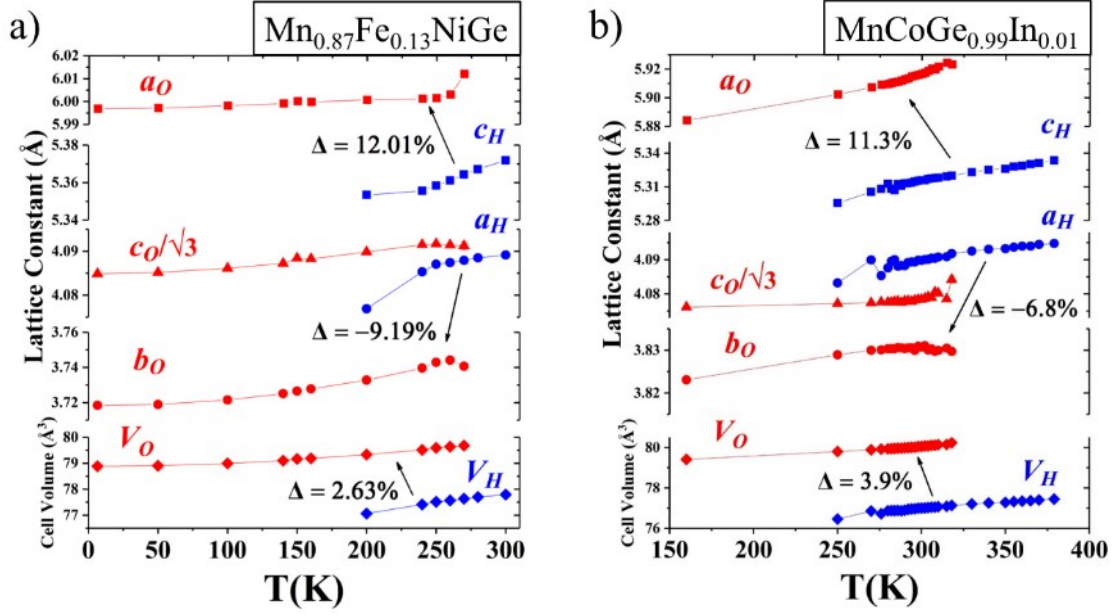


**Fig. S2** Variation of the specific lattice parameters and volume of hexagonal and orthorhombic structure with temperature for the free powders of (a)  $\text{Mn}_{0.87}\text{Fe}_{0.13}\text{NiGe}$  and (b)  $\text{MnCoGe}_{0.99}\text{In}_{0.01}$ .

For the details of magnetic and crystal structure during the martensitic transition, **Fig. S3a** typically shows the variable temperature NPD patterns for  $\text{Mn}_{1-x}\text{Fe}_x\text{NiGe}$  ( $x = 0.13$ ) collected at NIST Center for Neutron Research on the BT-1 high-resolution neutron powder diffractometer. The appearance of  $(000)^\pm$ , as well as the  $(101)^-$  and  $(101)^+$  magnetic satellites, at low temperature suggests the incommensurate magnetic phase [Ref. 34]. With increasing temperature, the peak intensities of  $(000)^\pm$  and orthorhombic  $(101)$  crystal reflection reduce and show a sharp drop around  $T_{mstru} \sim 256\text{K}$ . Meanwhile, the hexagonal  $(002)$  crystal reflection appears, which can be clearly seen in the inset of **Fig. S3a**. This result reveals that  $\text{Mn}_{1-x}\text{Fe}_x\text{NiGe}$  ( $x = 0.13$ ) undergoes a concurrent magnetic and structural transition around the  $T_{mstru}$  from paramagnetic hexagonal structure (space group:  $P6_3/mmc$ ) to the orthorhombic structure (space group:  $Pnma$ ) with incommensurate magnetic ordering. Moreover, the refinements of NPD pattern collected at 200K, as shown in **Fig. S3b**, indicate that all these magnetic reflections can be indexed by the propagation vector  $\mathbf{k} = [0.17357(3), 0, 0]$ , and  $\text{Mn}_{1-x}\text{Fe}_x\text{NiGe}$  ( $x = 0.13$ ) has a cone-spiral magnetic structure in martensite. The sketch is shown in the inset of **Fig. S3b**. Besides, the refinements also show that the magnetic moment localizes only on Mn/Fe sites with  $\mu(\text{Mn, Fe}) = 2.66(1) \mu_B$  (noting that we couldn't distinguish the moment of Fe from Mn atoms, as they occupy the same sites). The spiral axis lies along the a-axis, and the moment angle away from a-axis is  $70^\circ$ , showing a canted FM nature.

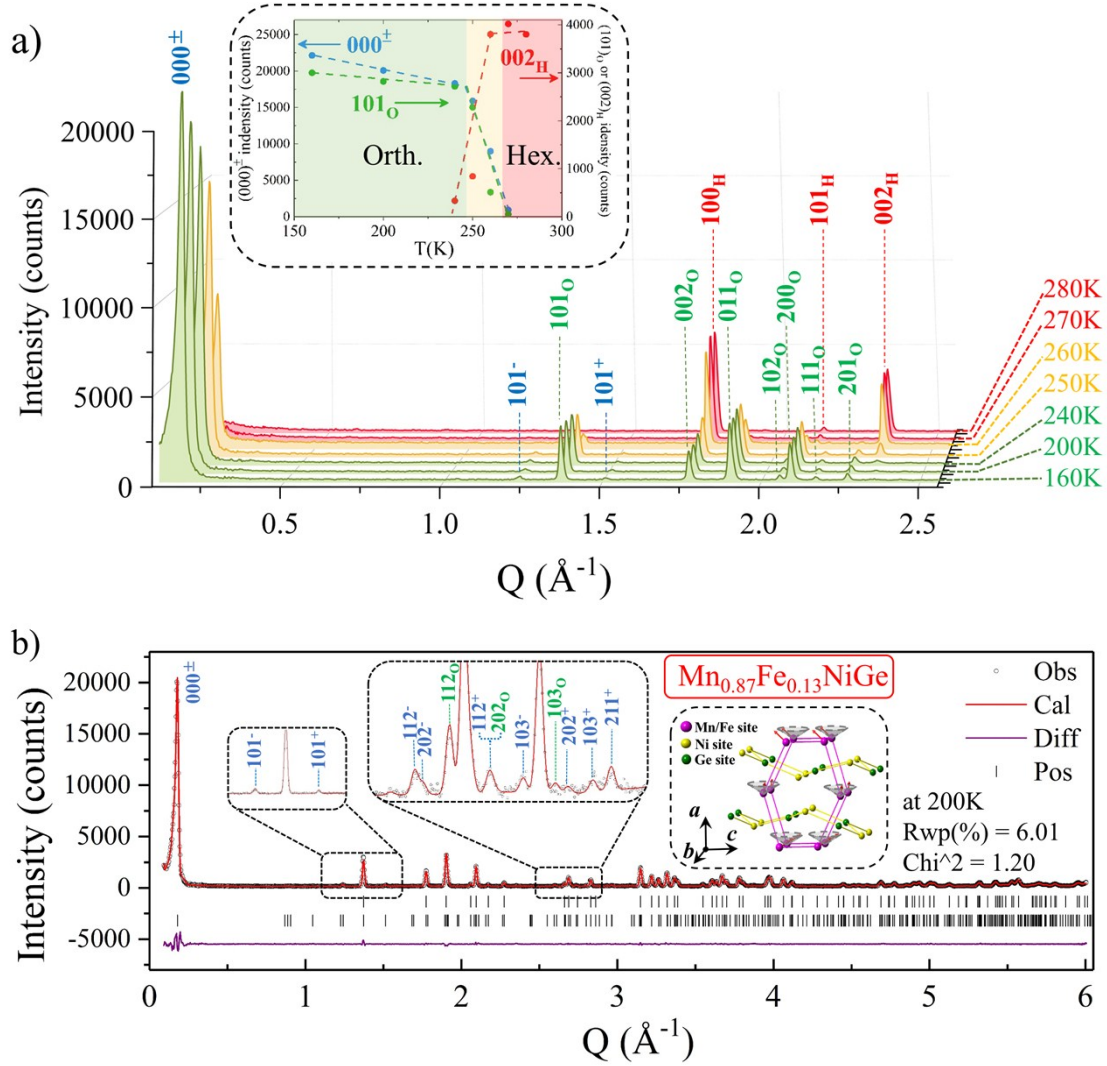


**Fig. S3** (a) Variable temperature NPD patterns of  $\text{Mn}_{1-x}\text{Fe}_x\text{NiGe}$  ( $x = 0.13$ ) collected from 160K to 280K, where the crystal reflections of orthorhombic and hexagonal phase and magnetic reflections are indexed. The inset shows the peak intensities of  $(000)^\pm$  magnetic reflection (blue dot), orthorhombic  $(101)$  (green dot) and hexagonal  $(002)$  (red dot) crystal reflections as a function of temperature. (b) Observed (black circle), calculated (red line) neutron diffraction patterns, their difference (purple line), peak position (black bar) for  $\text{Mn}_{1-x}\text{Fe}_x\text{NiGe}$  ( $x = 0.13$ ) collected at  $T = 200$  K by BT-1. The details of indexed magnetic reflections (marked by blue) are specially given in the left two insets, and the sketch of cone-spiral magnetic structure is given in the right inset.

The Fe-doped  $\text{MnNiGe}$  alloys in present work show similar anisotropy lattice distortion owing to the similar cone-spiral magnetic structure in martensite. To verify the cone-spiral magnetic structure for others. NPD studies were performed for another composition  $\text{Mn}_{1-x}\text{Fe}_x\text{NiGe}$  ( $x = 0.11$ ) with magnetostructural transition around  $T_{mstru} \sim 277\text{K}$ . The NPD patterns were collected at 180K by time-of-flight (TOF) general purpose powder diffractometer (GPPD) at CSNS in 3 ranges of low-Q, middle-Q and high-Q, as shown in **Fig. S4a**. Careful refinements indicate that all these magnetic reflections can be indexed by the propagation vector  $\mathbf{k} = [0.1788(2), 0, 0]$ , and the  $\text{Mn}_{1-x}\text{Fe}_x\text{NiGe}$  ( $x = 0.11$ ) has a cone-spiral magnetic structure similar to that of  $\text{Mn}_{1-x}\text{Fe}_x\text{NiGe}$  ( $x = 0.13$ ) shown above. Moreover, the refinements also show that the magnetic moment localizes only on Mn/Fe sites with  $\mu(\text{Mn, Fe}) = 2.57(3) \mu_B$  (noting that we couldn't distinguish the moment of Fe from Mn atoms, as they occupy the same sites). The spiral axis lies along the a-axis, and the moment angle away from a-axis is  $80^\circ$ , which is bigger than that of  $\text{Mn}_{1-x}\text{Fe}_x\text{NiGe}$  ( $x = 0.13$ ) (**Fig.**

S3).

The  $\text{Mn}_{1-x}\text{Fe}_x\text{NiGe}$  ( $x = 0.11$ ) shows similar distortion of local environments with  $d_1 = 3.191(2)$  Å,  $d_2 = 3.164(3)$  Å,  $\text{agl}_M = 143.7(2)^\circ$  in comparison with  $\text{Mn}_{1-x}\text{Fe}_x\text{NiGe}$  ( $x = 0.13$ ) mentioned above. For details, **Fig. S4d** displays the sketch of magnetic and crystal structure of  $\text{Mn}_{1-x}\text{Fe}_x\text{NiGe}$  ( $x = 0.11$  at 180K, 0.13 at 200K) in comparison with  $\text{MnCoGe}_{0.99}\text{In}_{0.01}$  (at 250K) in martensite. Calculations indicate that the former both show bigger  $\Delta_{\text{anis}}$  than the latter during the corresponding phase transitions, see details in **Table S1**.

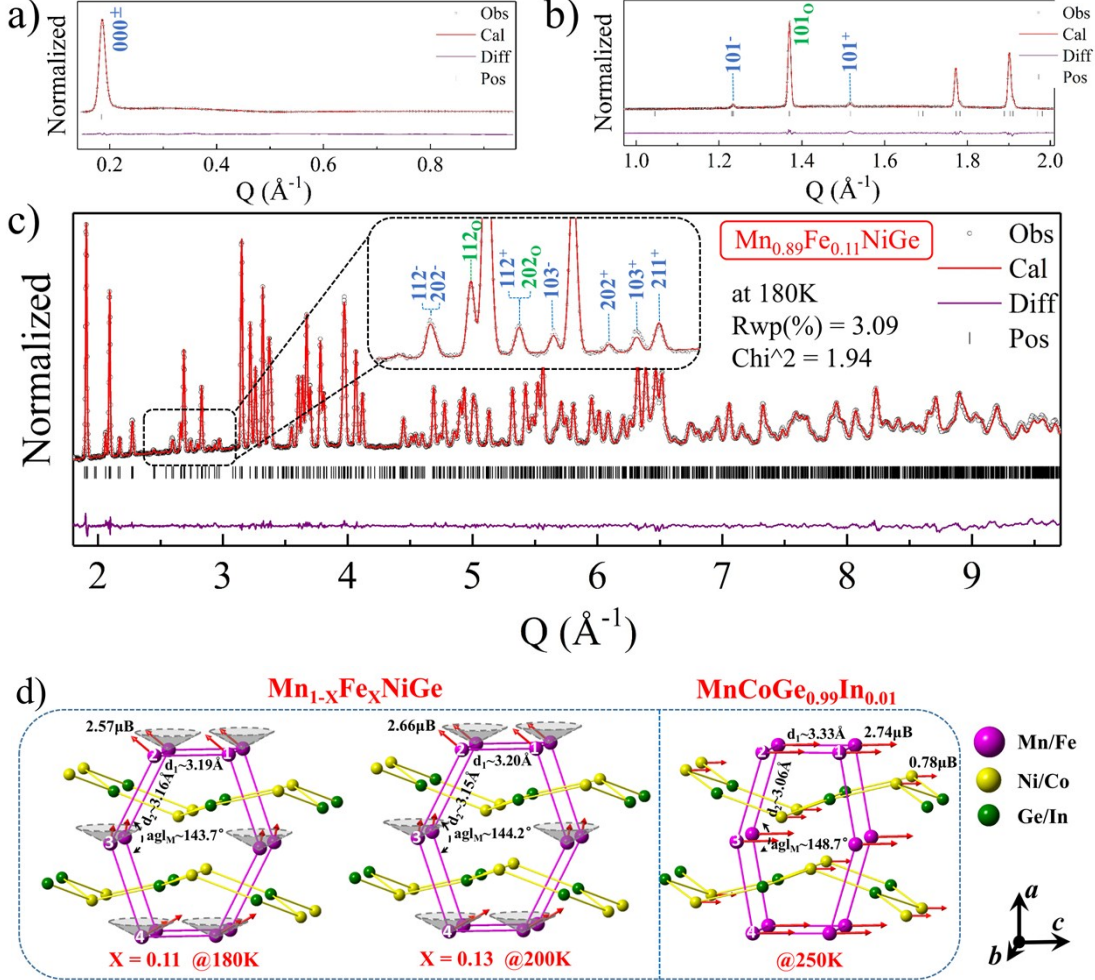


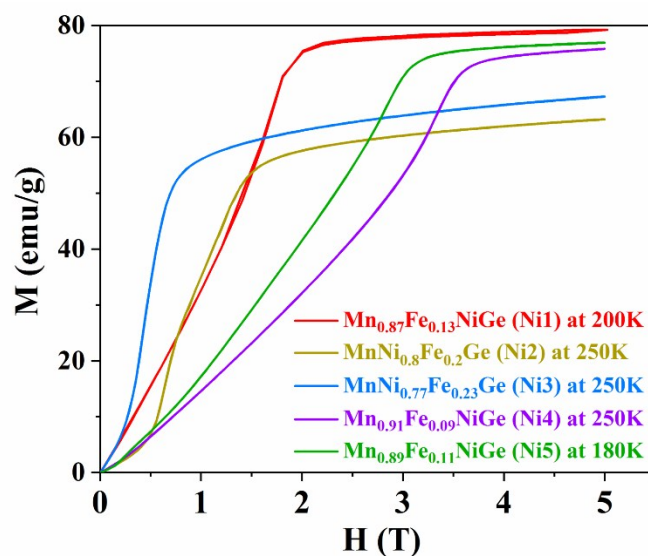
**Fig. S4** Observed (black circle), calculated (red line) neutron diffraction patterns, their difference (purple line), and peak position (black bar) for  $\text{Mn}_{1-x}\text{Fe}_x\text{NiGe}$  ( $x = 0.11$ ) collected at  $T = 180$  K in 3 ranges of (a) low-Q, (b) middle-Q, and (c) high-Q by GPPD. All the magnetic reflections are marked by blue, and the details of indexed magnetic reflections in the high-Q range are specially given in the inset. (d) The sketch of magnetic and crystal structure of  $\text{Mn}_{1-x}\text{Fe}_x\text{NiGe}$  ( $x=0.11$  at 180K, 0.13 at 200K) compared to  $\text{MnCoGe}_{0.99}\text{In}_{0.01}$  (at 250K) in martensite.

To see the magnetic performance of the cone-spiral magnetic structure against magnetic field, we measured the magnetization as a function of magnetic field (M-H) for the Fe-doped MnNiGe alloys at temperatures of martensite region, as shown in **Fig. S5**. The  $\text{Mn}_{1-x}\text{Fe}_x\text{NiGe}$  ( $x = 0.09, 0.11, 0.13$ ) and  $\text{MnNi}_{1-y}\text{Fe}_y\text{Ge}$  ( $y = 0.20, 0.23$ ) show martensitic magnetostructural transition ( $T_{mstru}$ ) at 308K, 277K, 256K, 310K, 295K, respectively. One can notice the regular evolution of cone-spiral magnetic structure with magnetic field. Initially, the magnetization increases approximately linearly with magnetic field, particularly for  $\text{Mn}_{1-x}\text{Fe}_x\text{NiGe}$  ( $x = 0.09, 0.11, 0.13$ ). This result indicates that the spiral angle gradually becomes smaller with increasing magnetic field and the moments rotate to be fully along a-axis at the saturated magnetic field. The saturated

magnetization is nearly the same for  $\text{Mn}_{1-x}\text{Fe}_x\text{NiGe}$  ( $x = 0.09, 0.11, 0.13$ ), equivalent to  $2.53\mu_B$ ,  $2.57\mu_B$ ,  $2.65\mu_B$  per Mn/Fe, respectively, which accords well with the refined moments from NPD at the corresponding temperatures for  $x = 0.11, 0.13$  (**Table S1**). Moreover, the saturated magnetic field monotonously increases with decreasing Fe doping, which also accords well with the refined results from NPD at the corresponding temperatures for  $x = 0.11, 0.13$ , noting that the refined spiral angle from a-axis is  $80^\circ, 70^\circ$ , respectively.

The stoichiometric  $\text{MnNiGe}$  displays a spiral AFM structure [Ref. 34], and the spiral axis also lies along the a-axis, which means the angle of moment from a-axis is  $90^\circ$ . The addition of Fe favors FM ordering, and the spiral angle gradually deviates from  $90^\circ$  with increasing the Fe content. So it is reasonable to speculate that  $\text{Mn}_{1-x}\text{Fe}_x\text{NiGe}$  with  $x = 0.09$  has similar cone-spiral magnetic structure and the spiral angle from a-axis is between  $80^\circ$  and  $90^\circ$ .

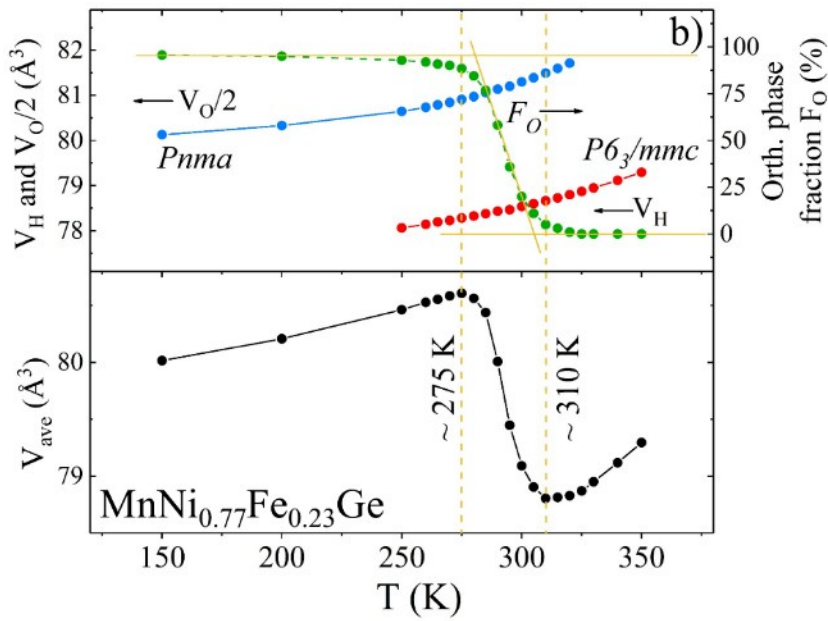
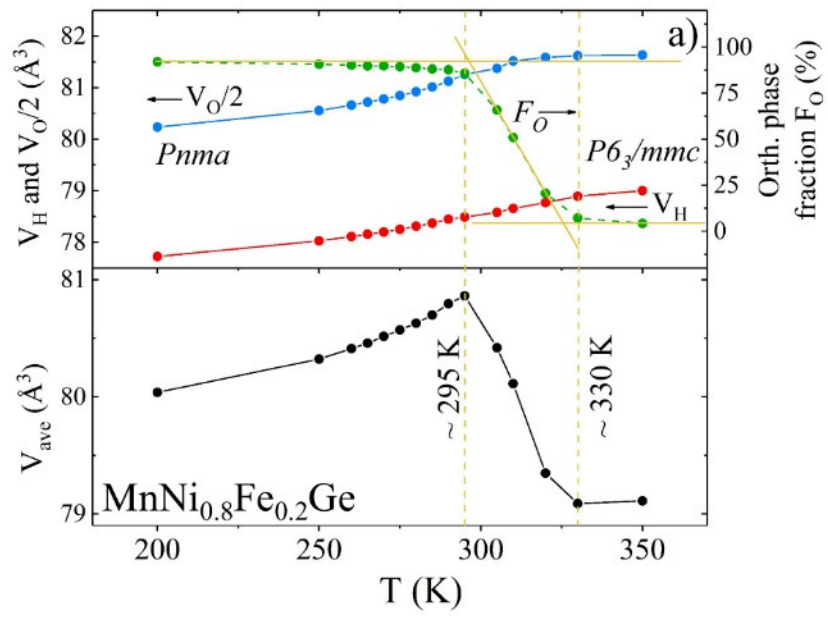
As for  $\text{MnNi}_{1-y}\text{Fe}_y\text{Ge}$  ( $y = 0.20, 0.23$ ), the initial magnetization with magnetic field is the same as that of  $\text{Mn}_{1-x}\text{Fe}_x\text{NiGe}$  ( $x = 0.09, 0.13$ ), though a metamagnetic transition occurs at  $0.5\text{T}$ ,  $0.2\text{T}$  respectively (see **Fig. S5**). Accordingly, similar cone-spiral magnetic structure in the absence of magnetic field can be speculated but details can be verified by NPD.



**Fig. S5** Magnetization as a function of magnetic field (M-H) for the Fe-doped  $\text{MnNiGe}$  alloys at temperatures of martensite region.

### III. The intrinsic crystallographic change during phase transition

From the refined lattice parameters and phase fractions, the evolution of unit cell volume with temperature for either hexagonal or orthorhombic phase was obtained, and then the average volume of lattice  $V_{ave}$  was deduced for the free powders. The results are shown in **Fig. S6**. It is noticeable that there is a increase of unit-cell volume during the martensitic transition from hexagonal to orthorhombic structure for all samples. The transition temperature ( $T_{mstru}$ ) is  $310\text{K}$ ,  $295\text{K}$ ,  $308\text{K}$  and  $256\text{K}$  for  $\text{MnNi}_{1-y}\text{Fe}_y\text{Ge}$  ( $y = 0.2, 0.23$ ) and  $\text{Mn}_{1-x}\text{Fe}_x\text{NiGe}$  ( $x = 0.09, 0.13$ ), respectively. For comparison, we defined the temperature window of NTE as the region where negative slope of  $V_{ave} - T$  occurs. For these free particles of  $\text{MnNi}_{1-y}\text{Fe}_y\text{Ge}$  ( $y = 0.2, 0.23$ ) and  $\text{Mn}_{1-x}\text{Fe}_x\text{NiGe}$  ( $x = 0.09, 0.13$ ), the width of NTE temperature window is  $35\text{K}$  ( $295\text{-}330\text{K}$ ),  $35\text{K}$  ( $275\text{-}310\text{K}$ ),  $50\text{K}$  ( $285\text{-}335\text{K}$ ) and  $40\text{K}$  ( $240\text{-}280\text{K}$ ), respectively. If isotropic expansion was supposed for the polycrystalline samples, the evaluated linear  $(\Delta L/L)_0 = (1/3) \Delta V_{ave}/V_{ave}$  would be  $7121, 7473, 7626, \text{ and } 7190 \times 10^{-6}$  in the temperature interval of  $40\text{K}$  ( $240\text{-}280\text{K}$ ),  $35\text{K}$  ( $295\text{-}330\text{K}$ ),  $35\text{K}$  ( $275\text{-}310\text{K}$ ), and  $50\text{K}$  ( $285\text{-}335\text{K}$ ), respectively.



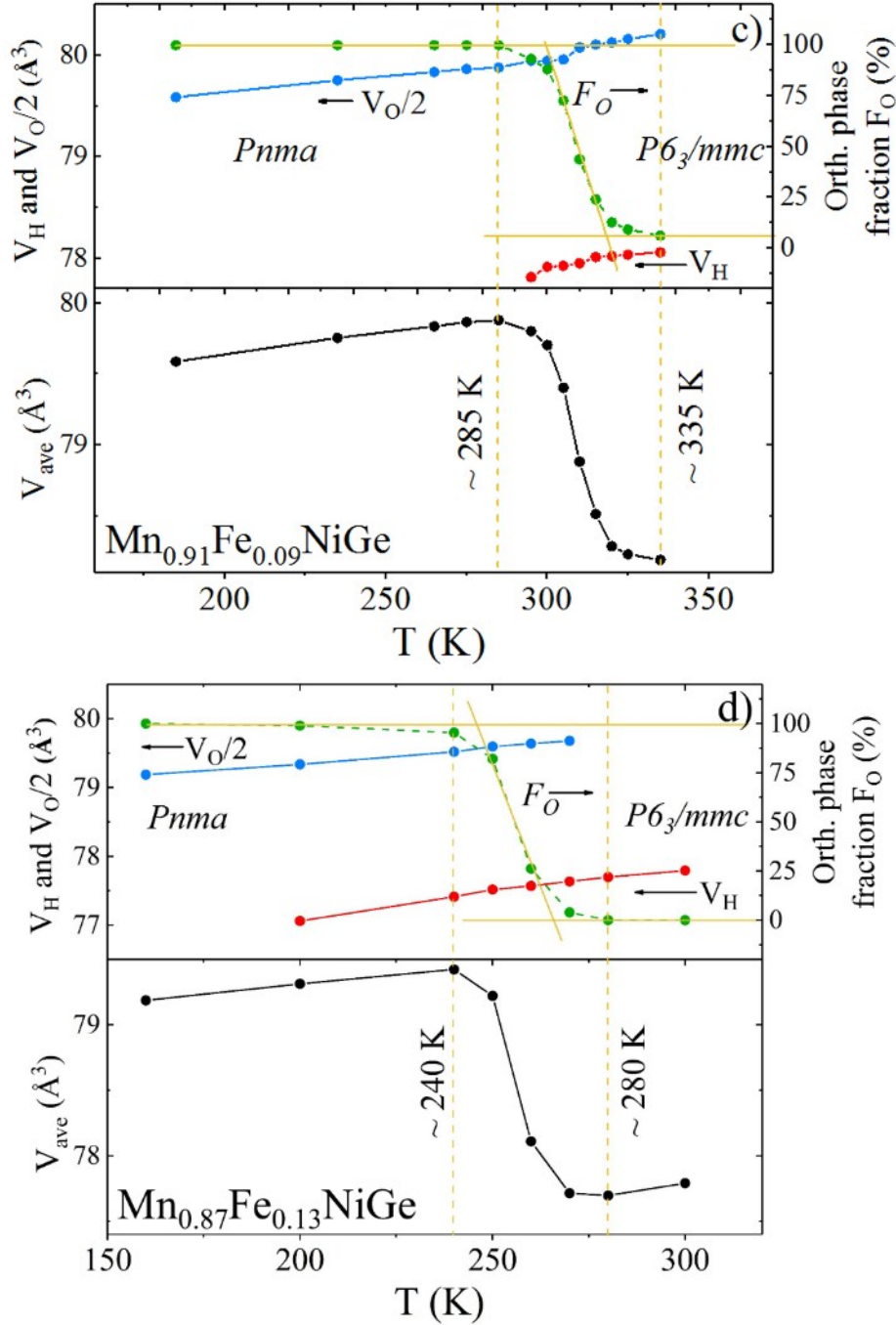


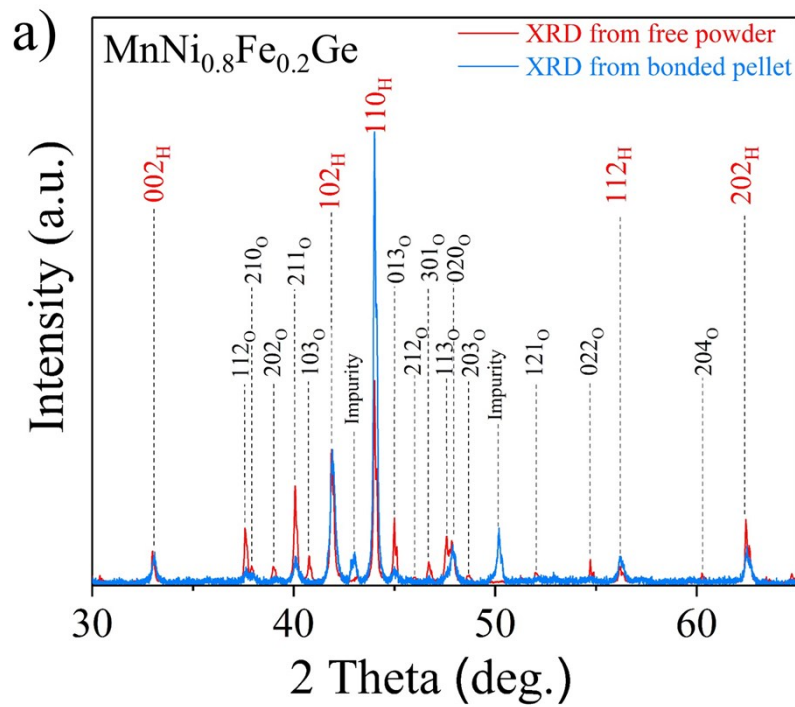
**Fig. S6** As the relationship between the unit-cell volume of hexagonal or orthorhombic phases is  $V_{\text{H}} \sim V_{\text{O}}/2$  [Ref. 28], the hexagonal unit cell volume  $V_{\text{H}}$  is compared with a half of the orthorhombic unit cell volume  $V_{\text{O}}/2$ . The upper panel of (a), (b), (c), and (d) shows unit cell volume of hexagonal phase ( $V_{\text{H}}$ , red solid circle), half of unit cell volume of orthorhombic phase ( $V_{\text{O}}/2$ , blue solid circle), and orthorhombic phase fraction ( $F_{\text{O}}$ , green solid circle) as a function of temperature for the free particle of  $\text{MnNi}_{1-y}\text{Fe}_y\text{Ge}$  ( $y = 0.2, 0.23$ ) and  $\text{Mn}_{1-x}\text{Fe}_x\text{NiGe}$  ( $x = 0.09, 0.13$ ), respectively. The lower panel presents the deduced average volume of lattice (black solid circle) as a function of temperature for the corresponding samples.

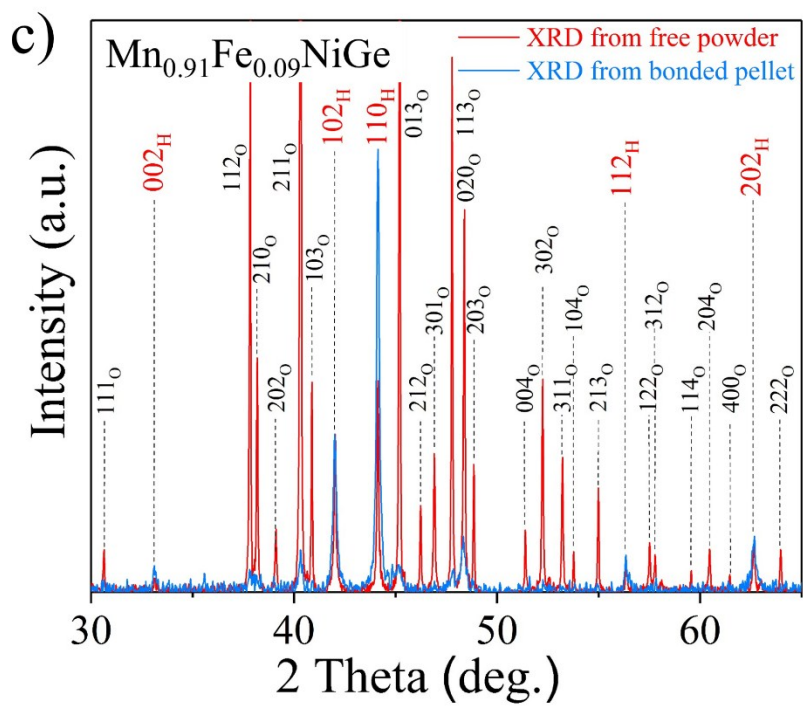
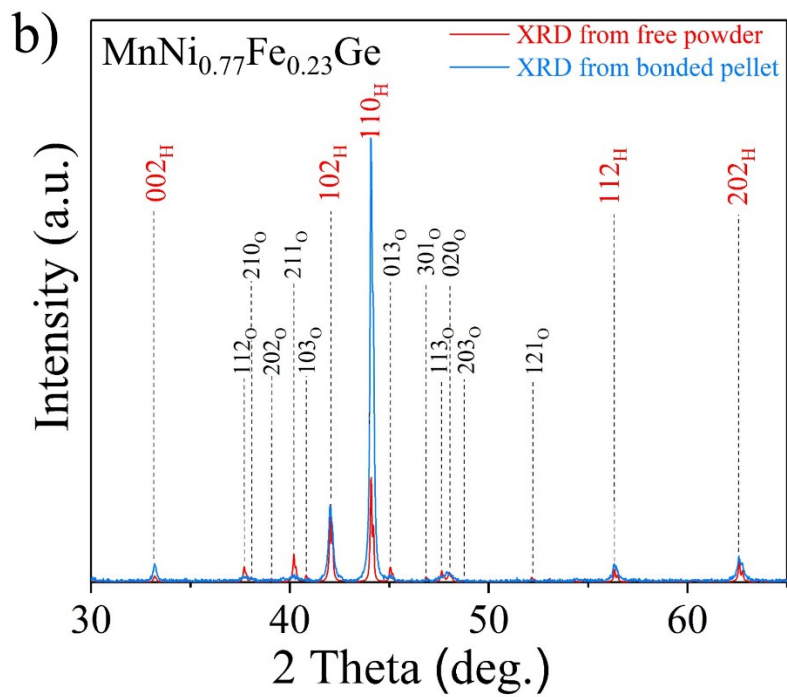
#### IV. Texture effect studied by XRD

To detect the degree of introduced texture in the bonded samples, we performed XRD measurements for the top surface of these bonded pellets (**Fig. 3c**). Through comparing the diffraction patterns with those from free powders (**Fig. S7**) collected at room temperature, the

degree of texture can be quantified by using Harris method [Ref. 40]. For the free powders of  $\text{MnNi}_{1-y}\text{Fe}_y\text{Ge}$  ( $y = 0.2, 0.23$ ) and  $\text{Mn}_{1-x}\text{Fe}_x\text{NiGe}$  ( $x = 0.09, 0.13$ ), the martensitic transition temperature ( $T_{mstru}$ ) is around room temperature for the former 3 samples. That is to say, the hexagonal phase coexists with orthorhombic phase at room temperature. For the bonded pellets, the introduced residual stress during bonding process often shifts the  $T_{mstru}$  to lower temperature [Ref. 29], and the Bragg peaks from orthorhombic phase would diminish at room temperature. So here we only consider the Bragg peaks of hexagonal structure in these diffraction patterns for calculating the orientation coefficient (OC).

**Fig. S7** (a), (b), (c), (d) and (e) exhibit the comparison of XRD patterns between free powders and bonded pellets for  $\text{MnNi}_{1-y}\text{Fe}_y\text{Ge}$  ( $y = 0.2, 0.23$ ),  $\text{Mn}_{1-x}\text{Fe}_x\text{NiGe}$  ( $x = 0.09, 0.13$ ), and  $\text{MnCoGe}_{0.99}\text{In}_{0.01}$ , respectively. For the free powders of  $\text{Mn}_{1-x}\text{Fe}_x\text{NiGe}$  ( $x = 0.09$ ) and  $\text{MnCoGe}_{0.99}\text{In}_{0.01}$ , the peaks of orthorhombic structure are strong as the  $T_{mstru}$  (308K for  $\text{Mn}_{1-x}\text{Fe}_x\text{NiGe}$  ( $x = 0.09$ ), 308K for  $\text{MnCoGe}_{0.99}\text{In}_{0.01}$ ) locates around room temperature. While for  $\text{Mn}_{1-x}\text{Fe}_x\text{NiGe}$  ( $x = 0.13$ ), the peaks of orthorhombic structure disappears because its  $T_{mstru} \sim 256\text{K}$  is lower than room temperature. For the same composition, the peak intensities from orthorhombic structure of bonded pellets are weaker than that of free powders, which can be understandable considering that the introduced residual stress during the molding process shifts the  $T_{mstru}$  to lower temperature [Ref.29].





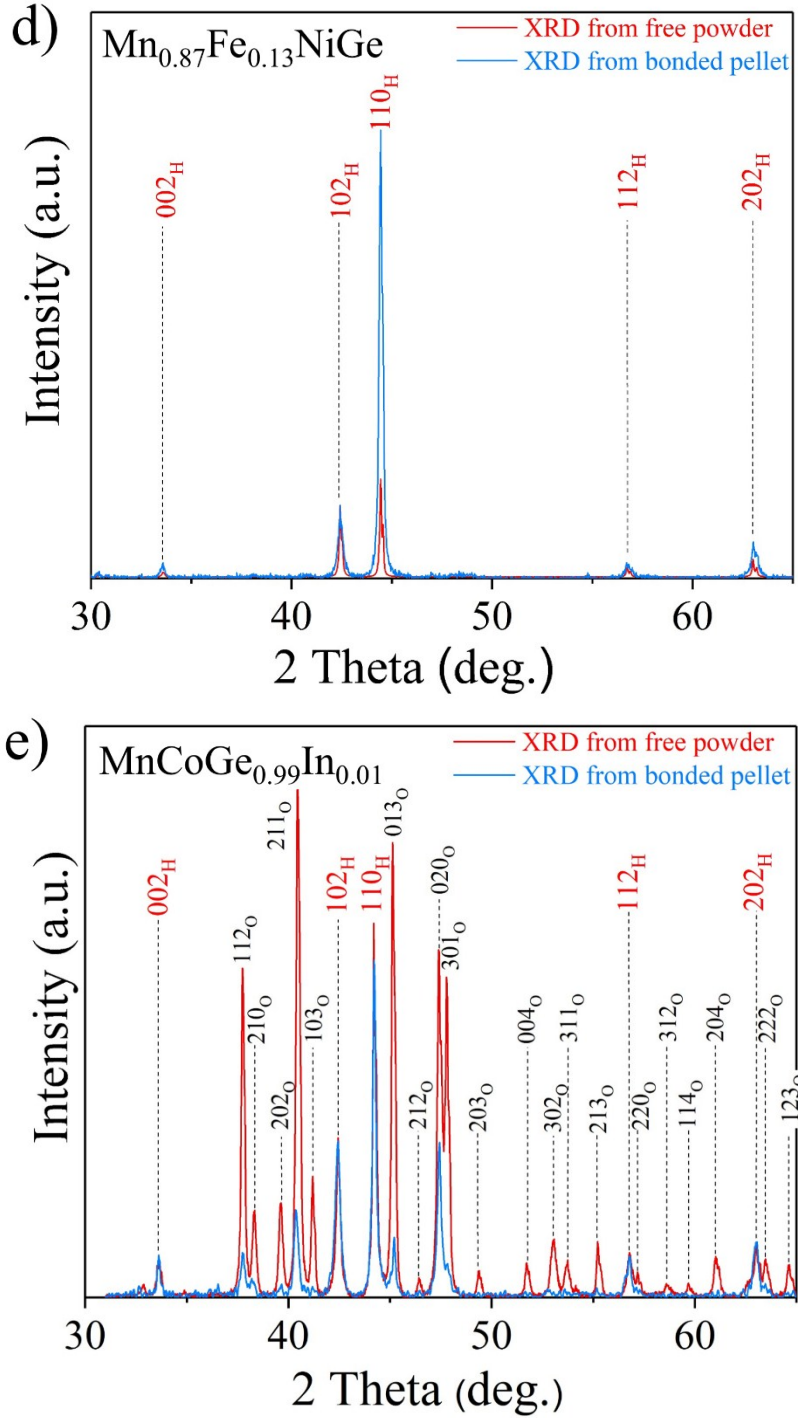


**Fig. S7.** (a), (b), (c), (d), and (e) show the comparison of XRD patterns between free powders (red line) and bonded pellets (blue line) for  $\text{MnNi}_{1-y}\text{Fe}_y\text{Ge}$  ( $y = 0.2, 0.23$ ),  $\text{Mn}_{1-x}\text{Fe}_x\text{NiGe}$  ( $x = 0.09, 0.13$ ) and  $\text{MnCoGe}_{0.99}\text{In}_{0.01}$ , respectively. All peaks are indexed, where the subscripts H and O represent hexagonal and orthorhombic phases, respectively.

### V. Numerical simulation of the enhanced $\Delta L/L$

To explore the enhanced NTE caused by preferred orientations of (110) and (002) crystal plane of the hexagonal structure, a numerical simulation is performed, where the orientation coefficient OC (110), OC (002) and  $(\Delta L/L)/(\Delta L/L)_0$  are set as  $x$ ,  $y$  and  $z$ , respectively ( $\Delta L/L$  is the measured value of bonded pellet and  $(\Delta L/L)_0$  is the crystallographic value). We fit these data by using the

following equation,

$$z = 2.126 \cdot x - 1.635 \cdot y + 0.5933 \quad (1)$$

It can be seen that the enhanced  $\Delta L/L$  has a positive correlation with the orientation of (110) crystal plane, while a negative correlation with the orientation of (002) crystal plane. That is to say, the bonded sample will be enhanced by the preferred orientation of the (110) crystal plane, while reduced by the preferred orientation of the (002) crystal plane. The functional images drawn according to the equation (1) are shown in **Fig. S8** (a) and (b). The experimental points roughly fall on the functional images, which illustrates that the equation (1) fits well with the experimental points. As the OC (002) = 1 was fixed, the OC (110) orientation would dominate the thermal expansion, and the  $(\Delta L/L)/(\Delta L/L)_0$  increases monotonously with varying the OC (110), implying the large enhancement of NTE.

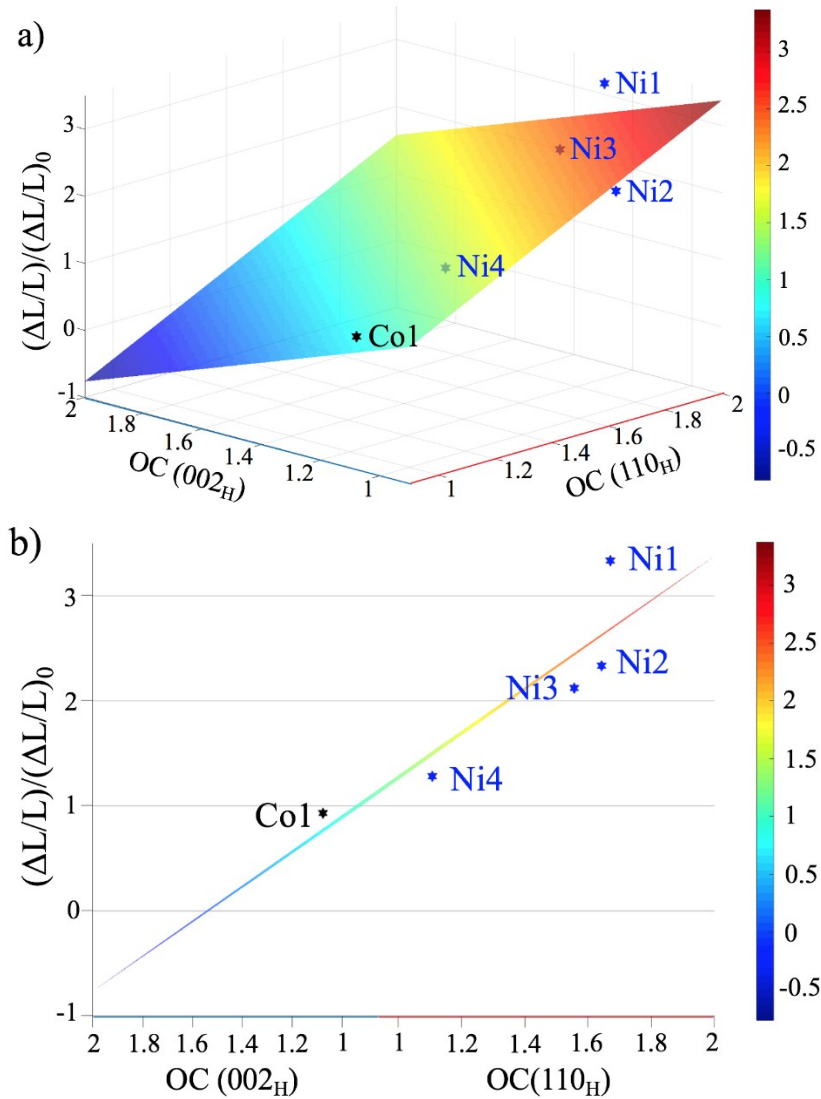


**Fig. S8.** The functional images (colorful plane) drawn according to the equation (1), where the orientation coefficient OC (110), OC (002), and  $(\Delta L/L)/(\Delta L/L)_0$  are set as x, y and z, respectively. (a) and (b) show the same simulated plane but from different viewpoints. Stars denote the experimental points for  $\text{Mn}_{0.87}\text{Fe}_{0.13}\text{NiGe}$  (Ni1),  $\text{MnNi}_{0.8}\text{Fe}_{0.2}\text{Ge}$  (Ni2),  $\text{MnNi}_{0.77}\text{Fe}_{0.23}\text{Ge}$  (Ni3),  $\text{Mn}_{0.91}\text{Fe}_{0.09}\text{NiGe}$  (Ni4), and  $\text{MnCoGe}_{0.99}\text{In}_{0.01}$  (Co1).

## VI. Broadening of NTE temperature range for bonded samples

For the  $\text{Ni}_2\text{In}$ -type hexagonal  $\text{MM}'\text{X}$  compounds ( $\text{M}$ ,  $\text{M}'$  = Transition element,  $\text{X}$  = Main element), the broadening of NTE temperature range of the bonded samples compared to the free powders involving martensitic structural transition can be ascribed to the introduced residual stress during molding process [Ref. 29; F. R. Shen, et al. *APL Mater.*, 2017, **5**, 106102]. The bonded samples experienced a high pressure of 1.35GPa during molding process before solidification at 170 °C. The residual stress introduced in the molding process cannot be released during the curing process, but remains possibly in the grain boundaries and micro-areas due to the adhesive action of the epoxy binder.

In our previous studies, the dependence of magnetization on temperature were compared between the bonded samples and free powders for MnCoGe-based compounds[Ref. 29]. Only the magnetostructural transition around  $T_{\text{mstru}}$  in MnCoGe<sub>0.99</sub> or the structural transition around  $T_{\text{stru}}$  in Mn<sub>0.97</sub>In<sub>0.03</sub>CoGe shifts and broadens for the bonded samples, while the pure magnetic transition at  $T_{\text{C}}$  remained unaffected. **Fig.S9** shows the compared dependence of magnetization on temperature between the bonded samples and free powders for Mn<sub>0.88</sub>Fe<sub>0.12</sub>NiGe. Similar broadening of NTE temperature range appears for the bonded samples around the  $T_{\text{mstru}}$ .

Previous investigations on Fe-doped MnNiGe indicated that the interlayer distance and the strengthening of covalent bonding between Mn-Mn atoms in the hexagonal structure plays a key role in stabilizing the hexagonal austenitic structure based on the valence-electron localization function (ELF) calculations [Ref.36]. We performed neutron powder diffraction (NPD) studies under pressure for the as-prepared powders MnCoGe<sub>0.99</sub>In<sub>0.01</sub> [Ref.30]. The results evidenced that the interlayer Mn-Mn distance is more sensitive to stress compared to the intralayer Mn-Mn distance. The rapidly shortening of the Mn-Mn interlayer distance caused by pressure strengthens the covalent bonding between Mn-Mn atoms and stabilizes the hexagonal austenitic structure, hence resulting in the shift of martensitic structural transition to lower temperature.

Note that the particle size of sample powders is not uniform, while the grain boundaries conducting the residual stress also have a distribution. Owing to the nonuniform characteristics, it can be understandable that the different particles suffer different residual stresses. Hence, the martensitic structural/magnetostructural transition of bonded samples shows broadening and shifting to lower temperature (**Fig.S9**).

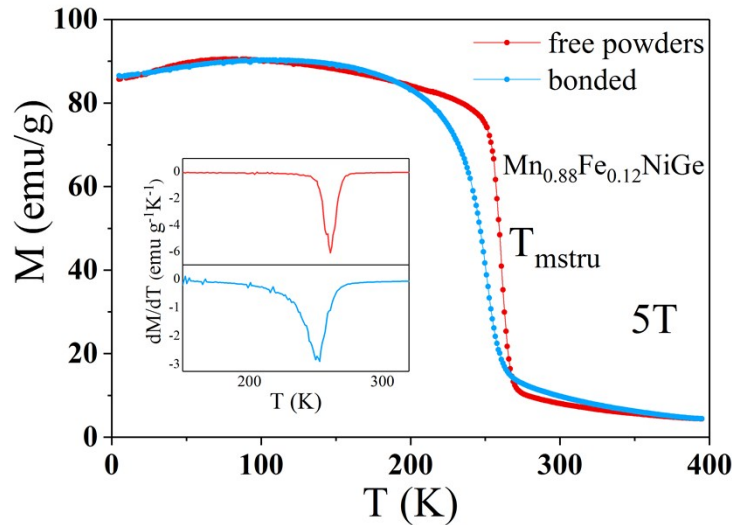


**Fig.S9** The comparison of temperature dependent magnetization between the bonded samples and free powders with magnetostructural phase transition  $T_{\text{mstru}}$  for Mn<sub>0.88</sub>Fe<sub>0.12</sub>NiGe. The insets show the corresponding  $dM/dT$  plots.

## VII. Enhancements of NTE studied in a single composition.

Fig.3a presents the enhanced NTE in different compositions with different particle sizes. To demonstrate the texture enhanced NTE for a single composition, we chose  $\text{Mn}_{0.88}\text{Fe}_{0.12}\text{NiGe}$  and studied the NTE behavior with particle size, as shown in **Fig.S10**. Much larger NTE was surprisingly observed, noting the maximal NTE magnitude  $\Delta L/L \sim 27487 \times 10^{-6}$  is 3.7 times larger than the crystallographic value  $(\Delta V/V)/3$  obtained by XRD for free powders, which even exceeds that ( $\sim 23690 \times 10^{-6}$ ) of Ni1. The SEM micrograph of corresponding free particles before bonding is also given in the right panel of **Fig.S10**. The enhanced ratio of NTE is mainly ascribed to texture effect, which can be controlled by particle size.

In our previous study, the particle size dependent NTE behavior for  $\text{MnCoGe}_{0.99}\text{In}_{0.01}$  with linear ferromagnetic (FM) structure was studied [F. R. Shen, et al. *APL Mater.*, 2017, **5**, 106102]. But we *never* observed a NTE exceeding the crystallographic contribution for samples with any particle size. As the particles were reduced down to (0.3–1 $\mu\text{m}$ ) by ball-milling, ultra-low thermal expansion appears due to the introduction of a large amount of amorphous structure.

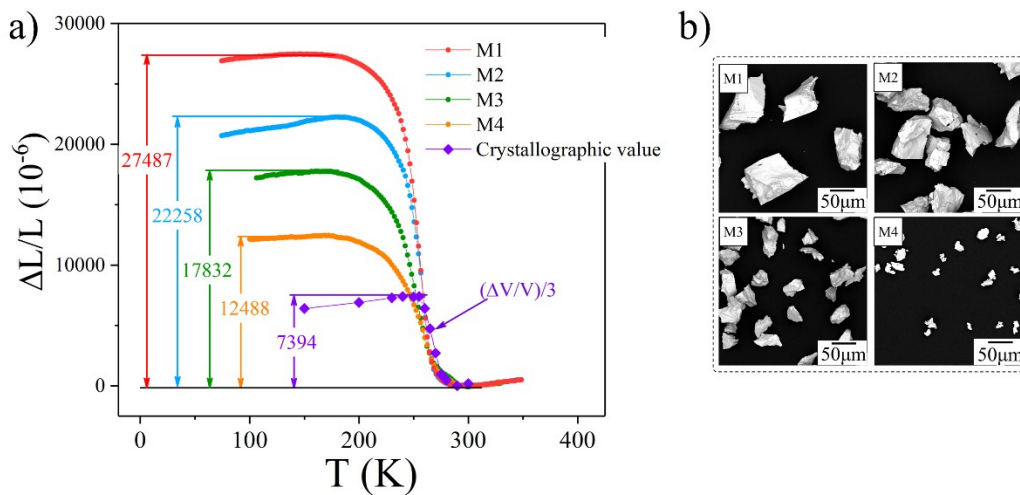


**Fig.S10** a) The measured linear  $\Delta L/L$  for the bonded  $\text{Mn}_{0.88}\text{Fe}_{0.12}\text{NiGe}$  with different particle sizes, in comparison to the crystallographic value  $(\Delta V/V)/3$ . b) The SEM micrograph of corresponding free particles before bonding. M1(80~100 $\mu\text{m}$ ), M2(60~80 $\mu\text{m}$ ), M3(20~50 $\mu\text{m}$ ), M4(10-30 $\mu\text{m}$ ).